

# Solving stress constrained problems in topology and material optimization

Michal Kočvara · Michael Stingl

Received: 21 September 2010 / Revised: 30 December 2011 / Accepted: 5 January 2012 / Published online: 8 February 2012  
© Springer-Verlag 2012

**Abstract** This article is a continuation of the paper Kočvara and Stingl (Struct Multidisc Optim 33(4–5):323–335, 2007). The aim is to describe numerical techniques for the solution of topology and material optimization problems with local stress constraints. In particular, we consider the topology optimization (variable thickness sheet or “free sizing”) and the free material optimization problems. We will present an efficient algorithm for solving large scale instances of these problems. Examples will demonstrate the efficiency of the algorithm and the importance of the local stress constraints. In particular, we will argue that in certain topology optimization problems, the addition of stress constraints must necessarily lead not only to the change of optimal topology but also optimal geometry. Contrary to that, in material optimization problems the stress singularity is treated by the change in the optimal material properties.

**Keywords** Topology optimization · Material optimization · Stress based design · Nonlinear semidefinite programming

## 1 Introduction

In our first article on this subject (Kočvara and Stingl 2007) we have introduced the concept of Free Material Optimization (FMO) and discussed formulations of stress constraints that would be computationally tractable and would lead to results consistent with physics. The same approach was also used for the standard problem of Topology Optimization (TO). We have introduced a numerical algorithm for the solution of the resulting finite dimensional optimization problems and presented several examples.

The present article results from further intensive study of this problem in the framework of the EU project PLATO-N (2006–2009).<sup>1</sup> First, we have developed a new optimization algorithm based on sequential convex optimization that allows us to solve much larger instances of the unconstrained problems. Further, we investigated several ways how to introduce the stress constraints in the problem in an efficient way. The results are presented here. The new algorithms allow us to solve large-scale two- and three-dimensional problems with stress local stress constraints. In the numerical section we present results of several examples containing stress singularity that stems from the initial geometry (re-entrant corner). While the topology optimization approach must necessarily lead to the removal of this singularity by changes in the geometry of the boundary of the optimal structure, the FMO result shows that the singularity is removed by the local properties of the optimal material.

---

This research was supported by the EU Commission in the Sixth Framework Program, Project No. 30717 PLATO-N, by the Academy of Sciences of the Czech Republic through grant No. A100750802, and by DFG cluster of excellence 315.

---

M. Kočvara (✉)  
School of Mathematics, University of Birmingham,  
Birmingham B15 2TT, UK  
e-mail: kocvara@maths.bham.ac.uk

M. Kočvara  
Institute of Information Theory and Automation,  
Academy of Sciences of the Czech Republic,  
Pod vodárenskou věží 4,  
18208 Praha 8, Czech Republic

M. Stingl  
Applied Mathematics II, University of Erlangen-Nuremberg,  
Nägelsbachstr. 49b, 91052 Erlangen, Germany  
e-mail: stingl@am.uni-erlangen.de

---

<sup>1</sup>[www.plato-n.org](http://www.plato-n.org)

We emphasize that we focus on the problem of free material optimization. The only topology optimization problem we consider is the Variable Thickness Sheet (VTS) problem (also called “free sizing problem”). This is to emphasize that, while mathematically very similar, these two problems (FMO and VTS) lead to completely different results when stress constraints are introduced. We do not consider the popular SIMP approach (e.g. Rozvany 2001a), as it brings another level of difficulty (loss of concavity in the dependence of the stiffness matrix on the design variable and the need to introduce some kind of filtering in the problem) and the SIMP problem is not really analogous to our primal problem which is FMO. There is a vast literature on the SIMP approach with stress constraints; see, e.g., Rozvany et al. (1992) or the recent article by Le et al. (2010) and the exhaustive list of references therein.

## 2 Primal FMO problem

### 2.1 Setting of the problem

Material optimization deals with optimal design of elastic structures, where the design variables are material properties. The material can even vanish in certain areas, thus one often speaks of topology optimization.

Let  $\Omega \subset \mathbb{R}^2$  be a two-dimensional bounded domain<sup>2</sup> with a Lipschitz boundary. By  $u(x) = (u_1(x), u_2(x))$  we denote the displacement vector at a point  $x$  of the body under load  $f$ , and by

$$e_{ij}(u(x)) = \frac{1}{2} \left( \frac{\partial u_i(x)}{\partial x_j} + \frac{\partial u_j(x)}{\partial x_i} \right) \quad \text{for } i, j = 1, 2$$

the (small-)strain tensor. We assume that our system is governed by linear Hooke’s law, i.e., the stress is a linear function of the strain

$$\sigma_{ij}(x) = E_{ijkl}(x)e_{kl}(u(x)) \quad (\text{in tensor notation}),$$

where  $E$  is the elastic stiffness tensor. The symmetries of  $E$  allow us to write the 2nd order tensors  $e$  and  $\sigma$  as vectors

$$e = (e_{11}, e_{22}, \sqrt{2}e_{12})^T \in \mathbb{R}^3,$$

$$\sigma = (\sigma_{11}, \sigma_{22}, \sqrt{2}\sigma_{12})^T \in \mathbb{R}^3.$$

<sup>2</sup>The entire presentation is given for two-dimensional bodies, to keep the notation simple. Analogously, all this can be done for three-dimensional solids.

Correspondingly, the 4th order tensor  $E$  can be written as a symmetric  $3 \times 3$  matrix

$$E = \begin{pmatrix} E_{1111} & E_{1122} & \sqrt{2}E_{1112} \\ & E_{2222} & \sqrt{2}E_{2212} \\ \text{sym.} & & 2E_{1212} \end{pmatrix}. \quad (1)$$

In this notation, Hooke’s law reads as  $\sigma(x) = E(x)e(u(x))$ .

For the elastic stiffness tensor  $E$  and given  $L$  independent external load functions  $f^\ell \in [L_2(\Gamma)]^2$  (where  $\Gamma$  is the part of boundary of  $\Omega$  that is not fixed by Dirichlet boundary conditions) the system is in equilibrium for a displacement function  $u^\ell$  which solves the weak equilibrium equations for  $\ell = 1, \dots, L$

$$\int_{\Omega} \langle E(x)e(u^\ell(x)), e(v(x)) \rangle dx - \int_{\Gamma} f^\ell(x) \cdot v(x) dx, \quad \forall v \in \mathcal{V} \quad (2)$$

where  $\mathcal{V} \subset [H^1(\Omega)]^2$  reflects the Dirichlet boundary conditions.

Consider the following optimization problem

$$\inf_{E, \rho, u \in \mathcal{V}} \int_{\Omega} g(E(x), \rho(x)) dx$$

subject to

$$\langle E(x)e(u^\ell(x)), e(v(x)) \rangle dx - \int_{\Gamma} f^\ell(x) \cdot v(x) dx, \quad (3)$$

$$\forall v \in \mathcal{V}, \ell = 1, \dots, L$$

$$\int_{\Gamma} f^\ell(x) \cdot u^\ell(x) dx \leq \gamma, \quad \ell = 1, \dots, L$$

$$\underline{\rho} \leq h(E(x), \rho(x)) \leq \bar{\rho}.$$

This problem can be interpreted as a minimum volume problem with a compliance constraint, where  $\int_{\Gamma} f(x) \cdot u(x) dx$  is the value of the compliance and  $\gamma$  the corresponding upper bound.

For different choices of  $E$  and  $\rho$  and functions  $g$  and  $h$ , we get different classes of problems:

- Free material optimization (FMO) (Zowe et al. 1997; Bendsøe and Sigmund 2002)

$$\rho \equiv 1, \quad E(x) \in \mathbb{S}^+ \text{ a.e. in } \Omega$$

$$g(\rho) = \text{tr}(E), \quad h(\rho) = \text{spectrum of } E \text{ at } x$$

where  $\mathbb{S}^+$  denotes the space of symmetric positive semidefinite matrices of proper dimension. The design variable is the elastic stiffness tensor  $E$  which is a function of the space variable  $x$  (see Bendsøe et al.

1994). The only constraints on  $E$  are that it is physically reasonable, i.e., that  $E$  is symmetric and positive semidefinite. As a “cost” of  $E$  we use the trace of  $E$ .

- Topology optimization (TO) with a given material

$$\rho \in L_\infty(\Omega), \quad E \equiv E_0$$

$$g(\rho) = h(\rho) = \rho$$

where  $E_0$  is the elasticity matrix of an isotropic material.

A particular case is the Variable Thickness Sheet (VTS) problem (Bendsøe and Sigmund 2002; Petersson 1996). Here  $\rho$  has the meaning of thickness of a two-dimensional isotropic elastic body. Another interpretation of the variable  $\rho$  is an artificial density. In such a case, we may try to avoid intermediate values by replacing  $\rho$  by  $\rho^p$  with increasing  $p$  and getting thus the SIMP approach; see Bendsøe and Sigmund (2002).

### 2.2 Discretization

Let  $m$  denote the number of finite elements and  $n$  the number of nodes. Depending on the type of the problem we solve, we either approximate  $\rho(x)$  by a function that is constant on each element, i.e., characterized by a vector  $\rho = (\rho_1, \dots, \rho_m)$  of its element values, or the matrix function  $E(x)$  by a function that is constant on each element, i.e., characterized by a vector of matrices  $E = (E_1, \dots, E_m)$  of its element values. We further assume that the displacement vector  $u(x)$  is approximated by a continuous function that is bilinear/trilinear on every element. Such a function can be written as  $u(x) = \sum_{i=1}^n u_i \vartheta_i(x)$  where  $u_i$  is the value of  $u$  at  $i$ -th node and  $\vartheta_i$  is the basis function associated with  $i$ -th node (for details, see Ciarlet 1978). At each node the displacement has  $dim$  components, so  $u \in \mathbb{R}^{dim \cdot n}$ . With the basis functions  $\vartheta_j, j = 1, \dots, n$ , we define  $(3 \times 2)$  matrices

$$\widehat{B}_j = \begin{pmatrix} \frac{\partial \vartheta_j}{\partial x_1} & 0 \\ 0 & \frac{\partial \vartheta_j}{\partial x_2} \\ \frac{1}{2} \frac{\partial \vartheta_j}{\partial x_2} & \frac{1}{2} \frac{\partial \vartheta_j}{\partial x_1} \end{pmatrix}.$$

Now, for the  $i$ -th finite element, let  $\mathcal{D}_i$  be an index set of nodes belonging to this element. Let  $nig$  denotes the number of Gauss integration points in each element. By  $B_{i,k}$  we denote the block matrix composed of  $(3 \times 2)$  blocks  $\widehat{B}_j$  at the  $j$ -th position,  $j \in \mathcal{D}_i$ , (evaluated at the  $k$ -th integration point) and zeros otherwise. Hence the full dimension of  $B_{i,k}$  is  $(3 \times 2n)$ .

The (global) stiffness matrix  $K$  is a sum of element stiffness matrices  $K_i$ :

$$K(E, \rho) = \sum_{i=1}^m \rho_i K_i(E), \quad K_i(E) = \sum_{k=1}^{nig} B_{i,k}^T E_i B_{i,k}.$$

After the discretization, problem (3) becomes

$$\min_{E, \rho, u \in \mathbb{R}^n} \sum_{i=1}^m g(E_i, \rho_i)$$

subject to

$$K(E, \rho)u^\ell = f^\ell, \quad \ell = 1, \dots, L$$

$$(f^\ell)^\top u^\ell \leq \gamma, \quad \ell = 1, \dots, L$$

$$\underline{\rho} \leq h(\rho_i) \leq \bar{\rho}, \quad i = 1, \dots, m$$
(4)

with variables  $(E_1, \dots, E_m) \in \mathbb{S}^+ \times \dots \times \mathbb{S}^+$  for the FMO problem or  $\rho \in \mathbb{R}^m$  for the TO problem.

Assuming that  $\underline{\rho} > 0$ , we can eliminate the displacement variable using the equilibrium equation  $u = K(E, \rho)^{-1} f$  to get the reduced primal problem:

$$\min_{E, \rho, u \in \mathbb{R}^n} \sum_{i=1}^m g(E_i, \rho_i)$$

subject to

$$(f^\ell)^\top K(E, \rho)^{-1} f^\ell \leq \gamma, \quad \ell = 1, \dots, L$$

$$\underline{\rho} \leq h(\rho_i) \leq \bar{\rho}, \quad i = 1, \dots, m.$$
(5)

### 3 Stress constraints

The motivation for our formulation of local stress constraints, together with references to the literature, have been discussed in detail in our previous paper (Kočvara and Stingl 2007). Let us just emphasize a point that is, in our opinion, very important.

#### 3.1 Stress or strain constraint?

It is well known that the stress/strain constraint problem may lead to serious numerical difficulties due to the effect of so-called vanishing constraints, see Achtziger and Kanzow (2007): The constraints may be active even in regions where the design variable tends to zero and which are then effectively void. This, in effect, leads to so-called singularity problem,<sup>3</sup> extensively studied in the structural

<sup>3</sup>Not to be confused with the singularity of the stress function, e.g., in the corner of an L-shaped domain.

optimization literature; see, e.g., Kirsch (1990), Cheng and Jiang (1992) and Rozvany (2001b). Whether or not we get this effect depends on the formulation of the constraint, the topology optimization model and, in particular, interpretation of the design variable. We will not concentrate on the solution of problems with vanishing constraints, as it requires special techniques, as described in Achtziger and Kanzow (2007). In our previous paper (Kočvara and Stingl 2007) we have presented an example demonstrating this effect in the contents of FMO.

### 3.1.1 Topology optimization

Let us first consider the topology optimization problem ( $E(x) = \rho(x)E_0$  with the variable  $\rho$ ). For an  $i$ th finite element and a  $k$ th integration point the formula for the discretized strain is given by

$$e_{i,k} = B_{i,k}u.$$

Clearly, the strain does not explicitly depend on the design variable and thus, if  $\rho_i \rightarrow 0$ , then  $e_{i,k}$  does not have to go to zero.<sup>4</sup> Hence, in this case, we will get a problem with vanishing constraints.

The formula for stress depends on our interpretation of the variable  $\rho$ . When  $\rho$  is interpreted as a thickness of a plate, then the stress is computed as

$$\sigma_{i,k} = E_0 B_{i,k}u.$$

We get exactly the same situation as above and again a problem with vanishing constraints.

If, on the other hand, we interpret  $\rho$  as an artificial density of the material, the stress is given by

$$\sigma_{i,k} = \rho E_0 B_{i,k}u.$$

Now the stress does depend on the design variable, which means that for  $\rho_i \rightarrow 0$  also  $\sigma_{i,k} \rightarrow 0$ . We may expect that this problem is much easier to solve numerically, as there are no vanishing constraints any more.

### 3.1.2 Free material optimization

In the FMO model ( $E(x)$  is the design variable), the strain is, obviously computed by the same formula as in the topology optimization problem, leading thus to a problem with vanishing constraints.

The stress, on the other hand is computed by the formula

$$\sigma_{i,k} = E B_{i,k}u$$

<sup>4</sup>Of course, the strain still depends on  $\rho$  implicitly, through  $u$ . However, this dependence does not force the strain to vanish when  $\rho$  tends to zero.

(we have no choice here). Again, the stress now explicitly depends on the design variable and we get an optimization problem *without* vanishing constraints.

## 3.2 Constraint formulation

In the continuous formulation, we would work with point-wise stresses, i.e., we would restrict the norm  $\|\sigma(x)\|$  for all  $x \in \Omega$ . However, in the finite element approximation we use the primal formula (working with displacements) and it is a well-known fact that, generally, evaluation of stresses (from displacements) at points may be rather inexact. Hence we will consider the following integral form of stress constraints

$$\int_{\Omega_i} \|\sigma\|_{vM}^2 \leq s_\sigma |\Omega_i|; \quad (6)$$

here  $\Omega_i$  is the  $i$ th finite element and  $|\Omega_i|$  its volume. The (semi)norm  $\|\cdot\|_{vM}$  (where “vM” stands for von Mises) is defined as

$$\|\sigma\|_{vM}^2 := \sigma^\top M \sigma, \quad \text{with } M = \begin{pmatrix} 2 & -1 & 0 \\ -1 & 2 & 0 \\ 0 & 0 & 3 \end{pmatrix}.$$

The upper bound  $s_\sigma > 0$  can be different for different load cases so, in general, we will consider bounds

$$s_\sigma^\ell, \quad \ell = 1, \dots, L.$$

The integrals will be further approximated by the Gaussian integration formulas, as in the finite element interpolation.

We will denote the stress in the  $i$ th element corresponding to  $\ell$ th load case by

$$\sigma_{i,\ell}(E, \rho) := \sum_{k=1}^{nig} \|E B_{i,k} K(E, \rho)^{-1} f^\ell\|_{vM}^2$$

hence the stress constraints will be written as

$$\sigma_{i,\ell}(E, \rho) \leq s_\sigma^\ell \bar{\rho}^2, \quad i = 1, \dots, m; \ell = 1, \dots, L. \quad (7)$$

## 3.3 Numerical treatment of stress constraints

We want to solve the reduced primal formulation (5). By adding the stress constraints to any of these formulations, we add many nonlinear constraints. This may cause serious problems in the behaviour of the respective algorithm and thus we need to treat these constraints carefully. In PENSCP, the following three different options have been implemented.

### 3.3.1 Direct treatment

Here we solve the original problem with all the new constraints directly, with no additional reformulation. That means, we solve the problem

$$\min_{E, \rho, u \in \mathbb{R}^n} \sum_{i=1}^m g(E_i, \rho_i)$$

subject to

$$(f^\ell)^\top K(E, \rho)^{-1} f^\ell \leq \gamma, \quad \ell = 1, \dots, L \tag{8}$$

$$\underline{\rho} \leq h(\rho_i) \leq \bar{\rho}, \quad i = 1, \dots, m$$

$$\sigma_{i,\ell}(E, \rho) \leq s_\sigma^\ell \bar{\rho}^2, \quad i = 1, \dots, m; \ell = 1, \dots, L.$$

The stress constraints are handled, just as the compliance constraint, by the sequential convex programming technique, as explained in Stingl et al. (2009a). Due to the large number of the stress constraints (the same as the number of finite elements), the computational complexity of the PENSCP algorithm grows rapidly. Hence this approach is only recommended for small to medium problems.

### 3.3.2 Direct treatment with active set strategy

An active set strategy is introduced in the PENSCP algorithm in order to reduce the computational effort needed to build the strictly convex separable approximations and solve the corresponding NLP. In the  $k$ -th iteration of PENSCP we fix a (small) threshold  $\eta > 0$  and discard any stress constraint with  $i = 1, \dots, m, \ell = 1, \dots, L$ , for which

$$\sigma_{i,\ell}(E, \rho) - s_\sigma^\ell \bar{\rho}^2 < -\eta.$$

Hence in the inner subproblems we only consider constraints that are  $\eta$ -active at the current iteration; all other constraints are ignored. This strategy is adopted also in the very first iteration.

This strategy may reduce the computational effort significantly if the number of active constraints at the optimum is low. Unfortunately, this is not the case of stress constraints. During the testing it turned out that for several examples from the academic test library there are many active stress constraints at the optimum—the amount of active constraints may vary from 5–30% of the total number of constraints. In these cases the active strategy does not bring the required speed up, as compared to the direct treatment.

Notice that similar difficulties caused by the large number of active constraints may be expected in methods based on augmented Lagrangians and general optimality criteria approach, such as the DCOC method by Zhou and Rozvany (1992, 1993).

### 3.3.3 Penalty approach

The most efficient way how to treat the stress constraints is to replace them by only one constraint. We can consider the following constraint that is fully equivalent to constraints (7):

$$\max_{\ell=1, \dots, L} \max_{i=1, \dots, m} (\sigma_{i,\ell}(E, \rho) - s_\sigma^\ell \bar{\rho}^2) \leq 0, \tag{9}$$

i.e., the  $\ell_\infty$ -type constraint. This is, however, a non-differentiable function and cannot be handled by the (smooth) PENSCP algorithm. We can use the standard approach and approximate the  $\ell_\infty$  norm by an  $\ell_p$  norm with big enough  $p$ . In the context of stress constrained topology optimization, this approach has been used, e.g. by Yang and Chen (1996), Duysinx and Sigmund (1997) and Le et al. (2010). Furthermore, to improve the conditioning, we can scale the constraint function by the log function and consider the following approximation of (9):

$$\log \sum_{\ell=1}^L \sum_{i=1}^m (\sigma_{i,\ell}(E, \rho) - s_\sigma^\ell \bar{\rho}^2)^p \leq 0. \tag{10}$$

However, neither this type of constraint delivered sufficient improvement in the efficiency of the PENSCP algorithm. Hence we opted for another standard idea from nonlinear optimization: replacing the constraints by a quadratic penalty term in the objective function. Thus, instead of solving problem (8), we solve a sequence of problems

$$\min_E \sum_{i=1}^m g(E_i, \rho_i) + \kappa \sum_{\ell=1}^L \sum_{i=1}^m \left( \max \left\{ 0, \left( \sigma_{i,\ell}(E, \rho) - s_\sigma^\ell \bar{\rho}^2 \right) \right\} \right)^2$$

subject to

$$(f^\ell)^\top K(E, \rho)^{-1} f^\ell \leq \gamma, \quad \ell = 1, \dots, L$$

$$\underline{\rho} \leq h(\rho_i) \leq \bar{\rho}, \quad i = 1, \dots, m \tag{11}$$

with increasing penalty parameter  $\kappa$ . Of course, unless we drive  $\kappa \rightarrow \infty$ , the solution of (11) will only be an approximation of the solution to (8). In particular, we cannot guarantee that the element-wise stress constraints are all feasible at the solution of (11). However, it is our experience that after 3–5 solutions of (11) with  $\kappa$  multiplied by 3 after each problem solution, we get a very good approximation to the solution of the original problem. Of course, the user can choose the initial value of  $\kappa$ , its update and the number of penalty updates.

Formulation (11) proved to be the most efficient one, in connection with the PENSCP solver. The examples presented in the next section were all solved using this formulation.

### 3.4 Sensitivity analysis

In the following, we describe how the sensitivities of each individual stress constraint  $\sigma_{i,\ell}(E, \rho)$  are computed. For simplicity, we restrict to the FMO case and omit the variable  $\rho$  in the rest of this paragraph. The partial derivative of  $\sigma_{i,\ell}$  w.r.t. an entry of the elastic stiffness tensor associated with element  $j$  (assuming  $i \neq j$ ) is given as

$$\begin{aligned} & \frac{\partial}{\partial(E_j)_{p,q}} \sigma_{i,\ell} \\ &= 2 \sum_{k=1}^{nig} \left( E_i B_{i,k} u^\ell \right)^\top M \left( E_i B_{i,k} K(E)^{-1} K_{j,p,q} u^\ell \right) \\ &= 2 \left( \sum_{k=1}^{nig} \left( E_i B_{i,k} u^\ell \right)^\top M E_i B_{i,k} \right) K(E)^{-1} K_{j,p,q} u^\ell, \end{aligned}$$

where  $K_{j,p,q}$  is defined as

$$K_{j,p,q} = \begin{cases} \sum_{k=1}^{nig} b_{j,k,p}^\top b_{j,k,q} & , \quad p = q, \\ \sum_{k=1}^{nig} b_{j,k,p}^\top b_{j,k,q} + b_{j,k,q}^\top b_{j,k,p} & , \quad p \neq q, \end{cases} \quad (12)$$

and  $b_{j,k,p}$  is the  $p$ -th row of  $B_{j,k}$ . In the case  $i = j$  an additional term

$$2 \sum_{k=1}^{nig} \left( E_i B_{j,k} \right)^\top M I_{p,q} B_{j,k} u^\ell,$$

with  $I_{p,q}$  being a matrix with 1 in position  $(p, q)$  and  $(q, p)$  and zeros otherwise is added. Obviously, when treating the stress constraints directly or in the framework of an active set approach, for each (active) constraint a system of the type  $K(E)v = d$  with  $d$  given as  $2 \sum_{k=1}^{nig} \left( E_i B_{i,k} u^\ell \right)^\top M E_i B_{i,k}$  has to be solved. For a large number of finite elements and consequently stress constraints, this can be prohibitive. The situation is different when using the penalty formulation outlined above. For convenience, we rewrite the penalized expression as

$$\hat{\sigma}_\ell(E) := \sum_{i=1}^m \varphi \left( \sigma_{i,\ell}(E) - s_\sigma^\ell \bar{\rho}^2 \right), \quad (13)$$

where  $\varphi$  is the smooth and convex function  $\max\{0, \cdot\}^2$ , and make use of the fact that the derivative of  $\hat{\sigma}_\ell$  with respect to the matrix variable  $E$  is given as

$$\nabla_E \hat{\sigma}_\ell(E) = \sum_{i=1}^m \varphi' \left( \sigma_{i,\ell}(E) - s_\sigma^\ell \bar{\rho}^2 \right) \nabla_E \sigma_{i,\ell}(E). \quad (14)$$

Taking this into account, we derive

$$\begin{aligned} & \frac{\partial}{\partial(E_j)_{p,q}} \hat{\sigma}_\ell(E) \\ &= 2 \left[ \sum_{i=1}^m \alpha_i \sum_{k=1}^{nig} \left( E_i B_{i,k} u^\ell \right)^\top M E_i B_{i,k} \right] K(E)^{-1} K_{j,p,q} u^\ell \\ & \quad + 2 \sum_{k=1}^{nig} \left( E_j B_{j,k} \right)^\top M I_{p,q} B_{j,k} u^\ell \end{aligned}$$

with coefficients  $\alpha_i = \varphi'(\sigma_{i,\ell}(E) - s_\sigma^\ell \bar{\rho}^2)$ . Thus only one linear system of the type  $K(E)v = d$  has to be solved for each load case. Note that the same idea can be applied when calculating the gradient of (10).

## 4 The PENSCLP algorithm

Here we present the basic steps of the PENSCLP algorithm together with the main convergence result. Full details can be found in Stingl et al. (2009b).

### 4.1 Basic problem statement

Our aim is to solve the following generic semidefinite program:

$$\begin{aligned} & \min_{Y \in \mathbb{S}} f_0(Y) \\ & \text{subject to} \\ & f_\ell(Y) \leq 0, \quad \ell = 1, 2, \dots, L, \\ & g_k(Y) \leq 0, \quad k = 1, 2, \dots, K, \\ & \underline{Y}_i \preceq_{\mathbb{S}^{d_i}} Y_i \preceq_{\mathbb{S}^{d_i}} \overline{Y}_i, \quad i = 1, 2, \dots, m \end{aligned} \quad (P)$$

with

$$\mathbb{S} = \mathbb{S}^{d_1} \times \mathbb{S}^{d_2} \times \dots \times \mathbb{S}^{d_m} \text{ and } (d_1, d_2, \dots, d_m) \in \mathbb{N}^m.$$

We assume that, in general,  $m$  is large ( $10^3$ – $10^5$ ) and  $d_i$  are small (2–10). That is, we have many small-size matrix variables and matrix constraints.

Throughout the section we make the following assumptions:

- (A1) The functions  $f_\ell : \mathbb{S} \rightarrow \mathbb{R}$ , ( $\ell = 0, 1, \dots, L$ ) are continuously differentiable.
- (A2) The functions  $g_k : \mathbb{S} \rightarrow \mathbb{R}$  ( $k = 1, 2, \dots, K$ ) are continuously differentiable, convex and separable with respect to the matrix variable  $Y$ .
- (A3) Problem (P) admits at least one solution.

Our main motivation is to solve the FMO and TO problems described in detail in Section 3. However, other applications can be found, e.g., in spline approximation (Alizadeh et al. 2008) and sparse SDP relaxation of polynomial optimization problems (Waki et al. 2006).

#### 4.2 A block-separable convex approximation scheme

In this section we briefly outline the concept of block separable convex approximations (see Stingl et al. 2009b) of continuously differentiable functions  $f : \mathbb{S} \rightarrow \mathbb{R}$ . We introduce the following convenient notation: Let  $I = \{1, 2, \dots, m\}$ . On  $\mathbb{S}$  we define the inner product  $\langle \cdot, \cdot \rangle_{\mathbb{S}} := \sum_{i \in I} \langle \cdot, \cdot \rangle_{\mathbb{S}^{d_i}}$ , where  $\langle \cdot, \cdot \rangle_{\mathbb{S}^{d_i}}$  is the standard inner product in  $\mathbb{S}^{d_i}$  ( $i \in I$ ). Moreover, we denote by  $\| \cdot \|_{\mathbb{S}}$  the norm induced by  $\langle \cdot, \cdot \rangle_{\mathbb{S}}$ . Finally, we denote the directional derivatives of  $f$  of first and second order in directions  $V, W \in \mathbb{S}$  by  $\frac{\partial}{\partial Y} f(Y; V)$  and  $\frac{\partial^2}{\partial Y \partial Y} f(Y; V, W)$ , respectively.

We start with the following definition:

**Definition 1** Let  $f : \mathbb{S} \rightarrow \mathbb{R}$  be continuously differentiable on a subset  $B \subset \mathbb{S}$  and  $\bar{Y} = (\bar{Y}_1, \bar{Y}_2, \dots, \bar{Y}_m) \in B$ . Moreover let *asymptotes*  $L = (L_1, L_2, \dots, L_m)^{\top}$ ,  $U = (U_1, U_2, \dots, U_m)^{\top}$  be given such that

$$L_i \prec_{\mathbb{S}_+^{d_i}} \bar{Y}_i \prec_{\mathbb{S}_+^{d_i}} U_i \text{ for all } i \in I$$

and  $\tau := \{\tau_1, \tau_2, \dots, \tau_m\}$  be a set of non-negative real parameters. Then we define the *hyperbolic approximation*  $f_{\bar{Y}}^{L,U,\tau}$  of  $f$  at  $\bar{Y}$  as

$$\begin{aligned} f_{\bar{Y}}^{L,U,\tau}(Y) := & f(\bar{Y}) + \sum_{i=1}^m \left\langle \nabla_+^i f(\bar{Y}), (U_i - \bar{Y}_i)(U_i - Y_i)^{-1} \right. \\ & \left. \times (U_i - \bar{Y}_i) - (U_i - \bar{Y}_i) \right\rangle_{\mathbb{S}^{d_i}} \\ & - \sum_{i=1}^m \left\langle \nabla_-^i f(\bar{Y}), (\bar{Y}_i - L_i)(Y_i - L_i)^{-1} \right. \\ & \left. \times (\bar{Y}_i - L_i) - (\bar{Y}_i - L_i) \right\rangle_{\mathbb{S}^{d_i}} \\ & + \sum_{i=1}^m \tau_i \left\langle (Y_i - \bar{Y}_i)^2, (U_i - Y_i)^{-1} \right. \\ & \left. + (Y_i - L_i)^{-1} \right\rangle_{\mathbb{S}^{d_i}}, \end{aligned} \tag{15}$$

where for all  $i \in I$  we define differential operators entry-wise by

$$\left( \nabla^i f \right)_{\ell,j} := \left( \frac{\partial f}{\partial Y_i} \right)_{\ell,j}, \quad 1 \leq \ell, j \leq d_i$$

and denote by  $\nabla_+^i f(\bar{Y})$  and  $\nabla_-^i f(\bar{Y})$  the projections of  $\nabla^i f(\bar{Y})$  onto  $\mathbb{S}_+^{d_i}$  and  $\mathbb{S}_-^{d_i}$ .

In Stingl et al. (2009b) it is proven that (15) is a convex approximation of  $f$  in the sense that the function value and partial (matrix) derivatives of  $f$  and  $f_{\bar{Y}}^{L,U,\tau}$  coincide at  $\bar{Y}$ ,  $f_{\bar{Y}}^{L,U,\tau}$  is strictly (matrix-) convex and block separable.

The formula (15) differs from the original formula in Stingl et al. (2009b) in the choice of the asymptotes. Here we restrict ourselves to only one (fixed) choice of asymptotes. The reason for this simplification is twofold. First it helps to unburden the notation. Second, and more important, there is no efficient dynamic choice of asymptotes known in the semidefinite programming case. This is in sharp contrast to the standard nonlinear programming situation; see Svanberg (1987), Fleury (1989), Bletzinger (1993) and Zillober (2001).

#### 4.3 A globally convergent algorithm based on hyperbolic approximations

Now we will use the local hyperbolic approximations defined in Section 4.2 in order to define an algorithm for the solution of the generic optimization problem (P).

Given an iteration index  $j$  and an associated feasible point  $Y^j$  of problem (P), we define local hyperbolic approximations of  $f_{\ell}$  ( $\ell = 0, 1, \dots, L$ ) as

$$f_{\ell}^j(Y) := (f_{\ell})_{Y^j}^{\tau_j}(Y) := (f_{\ell})_{Y^j}^{L,U,\tau_j}(Y),$$

and local approximations of (P) close to  $Y^j$  by replacing the objective and constraints in (P) by  $f_{\ell}^j(Y)$ , ( $\ell = 1, 2, \dots, L$ ), respectively.

Now we are able to present the basic algorithm for the solution of (P):

---

#### Algorithm 1

---

Let asymptotes  $L$  and  $U$  feasible with Definition 1 and a constant  $\vartheta > 1$  be given.

- (0) Find  $Y^1 \in F$ .
  - (1) Put  $j = 1$ .
  - (2) Choose  $\bar{\tau} \geq \tau_1^j, \tau_2^j, \dots, \tau_m^j \geq \underline{\tau} > 0$ .
  - (3) Solve problem  $(P^j)$ . Denote the solution by  $Y^+$ .
  - (4) If  $f_{\ell}^j(Y^+) \geq f_{\ell}(Y^+)$  for all  $\ell = 0, 1, \dots, L$ , GOTO (6).
  - (5) Put  $\tau_i^j \leftarrow \vartheta \tau_i^j$  for all  $i \in \left\{ \ell \in \{0, 1, \dots, L\} \mid f_{\ell}^j(Y^+) < f_{\ell}(Y^+) \right\}$  and GOTO (3).
  - (6)  $Y^{j+1} = Y^+$ .
  - (7) If  $Y^{j+1}$  is stationary for problem (P), STOP; otherwise put  $j = j + 1$  and GOTO (2).
-

An appropriate update scheme for the parameters  $\tau_i^j$  (step 2) will be proposed below, where we will also discuss algorithmic details as, for instance, a practical stopping criterion in step 7. There we will further point out, how we carry out step 0 above. For a detailed description of the algorithm applied to the solution of the subproblems arising from step 3, we refer again to Stingl et al. (2009b) and the references therein.

Algorithm 1 consists of *outer iterations* (steps 2–7) and *inner iterations* (steps 3–5). The inner iterations replace the line search used in the original algorithm stated in Stingl et al. (2009b). An interpretation of the inner iterations is as follows: Whenever the condition in step 4 fails to hold, we increase the influence of the strong convexity term. This results in a more conservative model. In a sense this is related to the trust region idea, which is a popular alternative to line search methods.

We now restate the central convergence result for Algorithm 1:

**Theorem 1** *Suppose that assumptions (A1)–(A3) are satisfied. Then, either Algorithm 1 stops at a stationary point of (P), or the sequence  $\{Y^j\}_j$  generated by Algorithm 1 has at least one accumulation point and each accumulation point is a stationary point of (P).*

For the proof, see Stingl et al. (2009b). To prove the convergence theorem, we have essentially followed the lines of the convergence proof in Svanberg (2002). Nevertheless all results needed to be restated in the semidefinite context.

## 5 Numerical experiments

### 5.1 Algorithmic details

*The choice of the asymptotes* As already mentioned in Section 4.2 we use fixed asymptotes. The following choice turned out to be robust:

$$L_i = 0, \quad U_i = 1.1 \bar{\rho} \text{Id},$$

where Id is the identity matrix in  $\mathbb{S}^3$  and  $\mathbb{S}^6$  for 2D- and 3D-problems, respectively.

*The subproblems* During all iterations, we solve the subproblems approximately. We use the following strategy: we start with a moderate accuracy of  $\varepsilon = 10^{-3}$  for the KKT error of the subproblem. During the outer iterations we adjust the tolerance according to the current KKT error of the master problem.

*The choice of  $\tau$*  The parameters  $\tau_i^j$  ( $i \in I$ ) in the  $j$ -th outer iteration are initialized such that the following condition is valid:

$$-\nabla^i f_\ell(E^j) + \tau_i^j I \succeq \delta I \quad (i \in I)$$

for all  $i \in I$  and all  $\ell = 0, 1, \dots, L$ . A typical choice for  $\delta$  is  $10^{-4}$ . The constant update factor  $\vartheta$  used in step 4 of Algorithm 1 is typically chosen from the interval  $[2, 10]$ . For a more sophisticated update scheme we refer to Svanberg (2002).

*A practical stopping criterion* We use two stopping criteria for Algorithm 1. The first one is based on the relative difference of two successive objective function values. We consider this stopping criterion as achieved if the relative difference falls below some given threshold  $\epsilon_1$  (typically  $\epsilon_1 = 10^{-8}$ ). The second stopping criterion is based on the following KKT-related error measures:

$$\begin{aligned} \text{err}_1 &= \left\| \nabla L(Y^l, y^l, u^l, \underline{U}^l, \bar{U}^l) \right\|, \\ \text{err}_2 &= \max \left\{ f_\ell(Y^l), g_k(Y^l) \mid \ell = 1, 2, \dots, L, k = 1, 2, \dots, K \right\}, \\ \text{err}_3 &= \max \left\{ |y_\ell^l f_\ell(Y^l)|, |u_k^l g_k(Y^l)|, \right. \\ &\quad \left. |\langle \underline{U}_j^l, Y_j^l - \underline{Y}_j \rangle|, |\langle \bar{U}_j^l, \bar{Y}_j - Y_j^l \rangle| \mid \right. \\ &\quad \left. \ell = 1, \dots, L, k = 1, \dots, K, j = 1, \dots, m \right\}, \end{aligned}$$

where  $Y^l$  is the approximate solution at iterate  $l$ ,  $L$  is the Lagrangian associated with problem (P) and  $y^l, u^l, \underline{U}^l$  and  $\bar{U}^l$  are the corresponding vectors of Lagrangian (matrix) multipliers associated with the constraint functions  $f_\ell, g_k$  and the lower and upper matrix bound constraints, respectively. Recall that the feasibility of  $Y^l$  w.r.t. the matrix bound constraints is maintained throughout all iterations. Now we define our second stopping criterion as

$$\frac{1}{3} \sum_{i=1}^3 \text{err}_i \leq \epsilon_2, \tag{16}$$

where a typical value for  $\epsilon_2$  is  $5 \cdot 10^{-5}$ .

**Fig. 1** L-shaped domain: geometry, load and boundary conditions

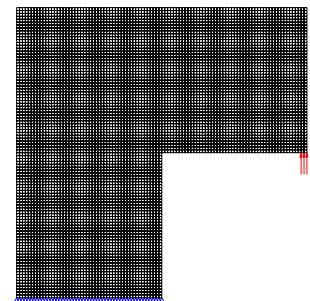


**Fig. 2** Problem TC04-s4, FMO, no stress constraints. Trace of the optimal material (*top-left*), von Mises stress (*top-right*), principal stress directions (*bottom-left*), zoom on the re-entrant corner (*bottom-right*)

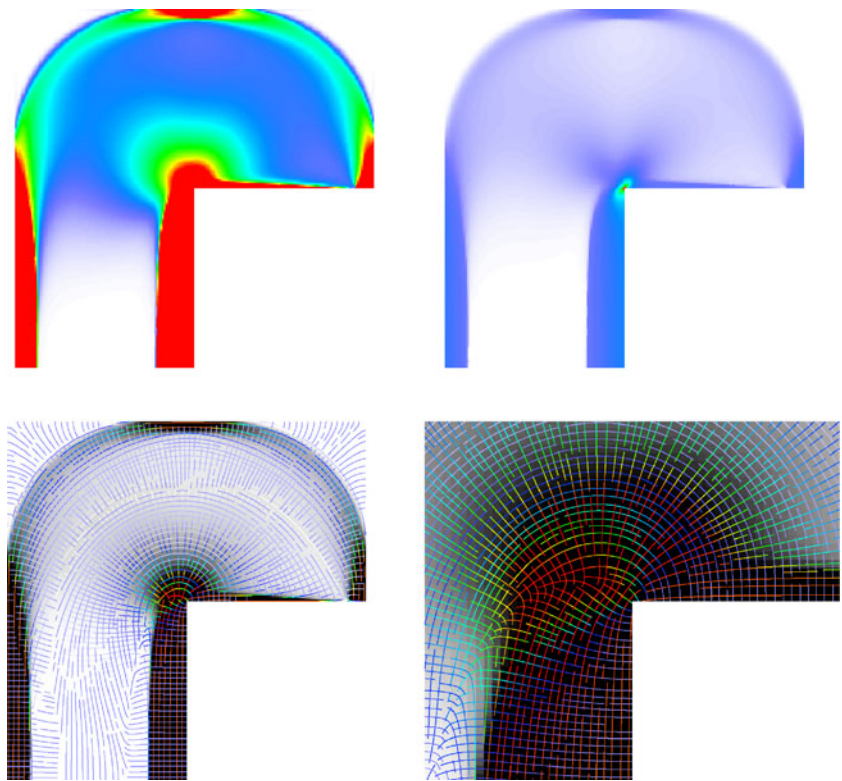


**Fig. 3** Problem TC04-s4, FMO, stress constraints. Trace of the optimal material (*top-left*), von Mises stress (*top-right*), principal stress directions (*bottom-left*), zoom on the re-entrant corner (*bottom-right*)

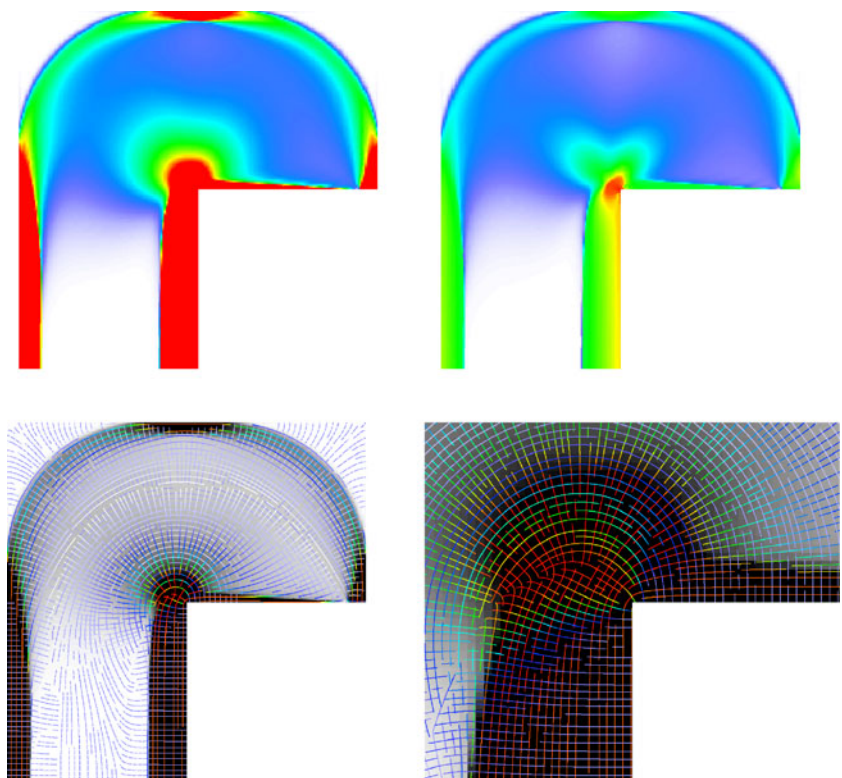
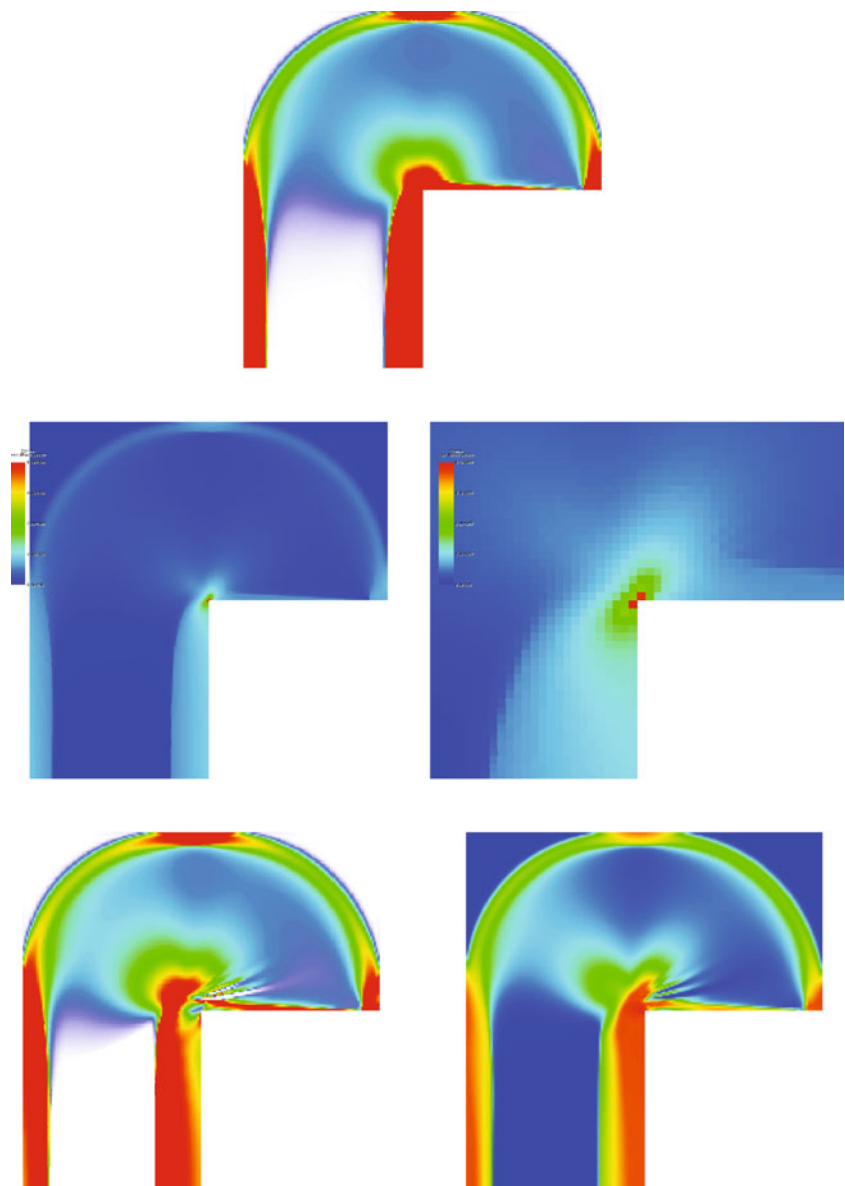


**Fig. 4** Problem TC04-s4, VTS, without and with stress constraints. Optimal  $\rho$  for the unconstrained problem (*top-center*), the corresponding stress (*mid-left*), zoom on the stress at the re-entrant corner (*mid-right*),  $\rho$  for the stress constrained problem (*bottom-left*) and the corresponding stresses (*bottom-right*)



*How to find an initial feasible point?* We use the following strategy inspired by Zillober (2001): If no feasible point is known, we start by solving the following auxiliary problem:

$$\min_{Y \in \mathbb{S}} f_0^j(Y) + \sum_{\ell=1, \dots, L} \eta_\ell f_\ell^j(Y)$$

subject to

$$g_k(Y) \leq 0, \quad k = 1, 2, \dots, K,$$

$$\underline{Y}_i \preceq_{\mathbb{S}^{d_i}} Y_i \preceq_{\mathbb{S}^{d_i}} \bar{Y}_i, \quad i = 1, 2, \dots, m.$$

Here the parameters  $\eta_\ell$ ,  $\ell = 1, 2, \dots, L$ , are penalty parameters, which are increased until a feasible solution is identified.

*The code* We have implemented the algorithm in the C programming language. In what follows we refer to the resulting code as PENSCLP. All FMO and TO computations have been carried out by the software platform PLATO-N.

## 5.2 Numerical examples

The classic example for testing the effect of stress constraints is the L-shaped domain; see Fig. 1. When made of homogeneous isotropic material, the structure exhibits a stress singularity at the peak of the re-entrant corner. If we transform the problem to a local radial coordinate system, located at this corner, the radial stress components would go to infinity when approaching the origin. In the global Cartesian coordinate system, the norm of the stress tensor goes to infinity as we approach the re-entrant corner. When we

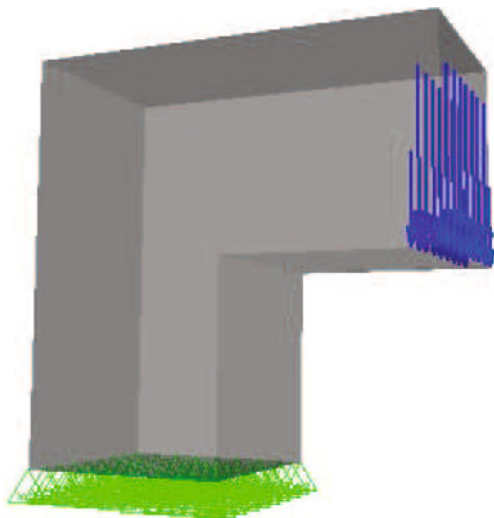
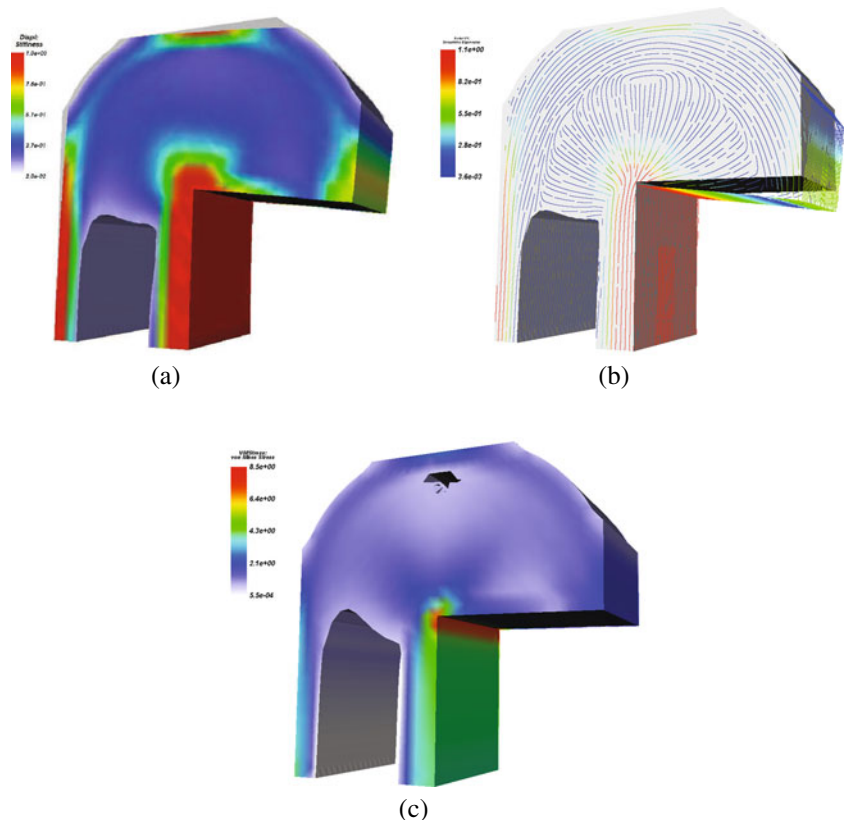


**Fig. 5** Problem TC13-s3, geometry and forces

solve the discretized problems with a homogeneous mesh, the stress would only go to infinity when the mesh size parameter goes to zero. For fixed mesh size, however, the stress values still reach much bigger values at the elements neighboring the corner than in the rest of the domain.

**Fig. 6** Problem TC13-s3, no stress constraints: **a** material density & deformed geometry; **b** principal material orientation; **c** stress distribution

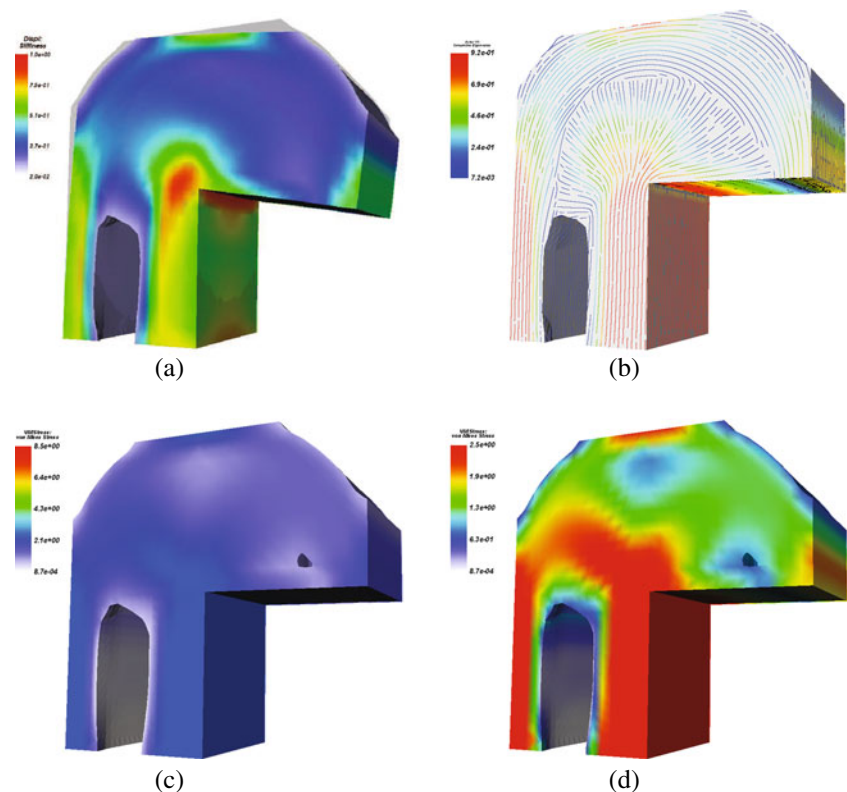


In all numerical examples, we first solve the problem without stress constraints. From the solution of the unconstrained problem we obtain the maximal stress and, based on that, select the stress upper bound for the constrained problem. The stress constrained problem is then solved with the same data. Notice that the compliance constraint is essential even in the presence of the stress constraints. In the absence of the compliance constraint the material in most finite elements would be on the lower bound and the optimal structure would not have any practical sense. The upper bound on the compliance was chosen such that the optimal objective function value is about 0.3 in all examples.

All examples below were solved on a single core of a standard PC with a tact frequency 2.83 GHz and 8 Gbyte memory.

*Example 1 (TC04-s4, FMO)* We first solved the FMO problem discretized by 30 000 finite elements without the stress constraints (problem TC04-s4 in the academic test library). The upper bound for compliance was 8,500. The PENSCP code needed 295 iterations and 51 min 43 s CPU time to reach an objective value (total stiffness) of 0.3321. The optimal solution was feasible. The trace of the optimal material is depicted in Fig. 2 (top-left) while the von Mises stress in each element is shown in the top-right figure. The maximal stress of 5.7 was obviously reached in the two corner

**Fig. 7** Problem TC13-s3 with stress constraints: **a** material density & deformed geometry; **b** principal material orientation; **c** stress distribution; **d** stress distribution—active set



elements. Figure 2 bottom-left and bottom-right show the corresponding principal stress directions and the zoom on the re-entrant corner, respectively. As the material in most elements is orthotropic, these directions also corresponds to the directions of orthotropy.

Next we have solved the same example again with compliance bound 8,500, this time with the stress constraints. The upper stress bound was chosen  $s_\sigma = 2.0$ . We solved a sequence of four problems (11) with increasing value of the penalty parameter  $\kappa$ . The total CPU time was 5 h 20 min 7 s. The final value of the highest stress was 2.00034 and value of the objective 0.3602. The results are depicted in Fig. 3, with the same meaning as in the unconstrained case. When comparing the unconstrained and the stress constrained results, we can see that there is hardly any change in the trace of the optimal material. There are, however, changes in the principal stress directions. So the stress concentration is “smoothened” by different properties of the material in the neighborhood of the re-entrant corner, rather than by changes in the geometry.

For the VTS problem (where the material properties are fixed and we just design the multiplier of the material matrix  $\rho \in \mathbb{R}^m$ ), the only way to remove the stress singularity is to change the geometry of the domain, in particular, to replace the sharp corner by a sort of smooth arc. The next example will demonstrate this.

*Example 2 (TC04-s4, VTS)* We solve the same problem as above, this time using the VTS model. Figure 4 shows the results. First we the distribution of the optimal  $\rho$  for the unconstrained problem (top-center), then the corresponding

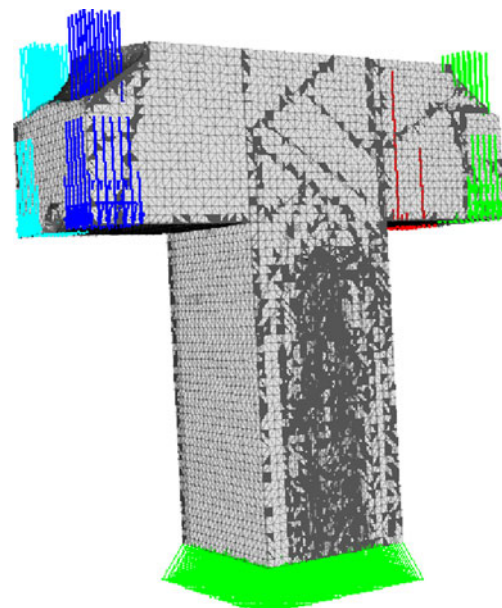


**Fig. 8** Problem TC11-s4—geometry and forces

**Fig. 9** Problem TC11-s4, no stress constraints: **a** material density & deformed geometry (first load case); **b** stress distribution; **c** principal material orientation; **d** principal material orientation (zoom)

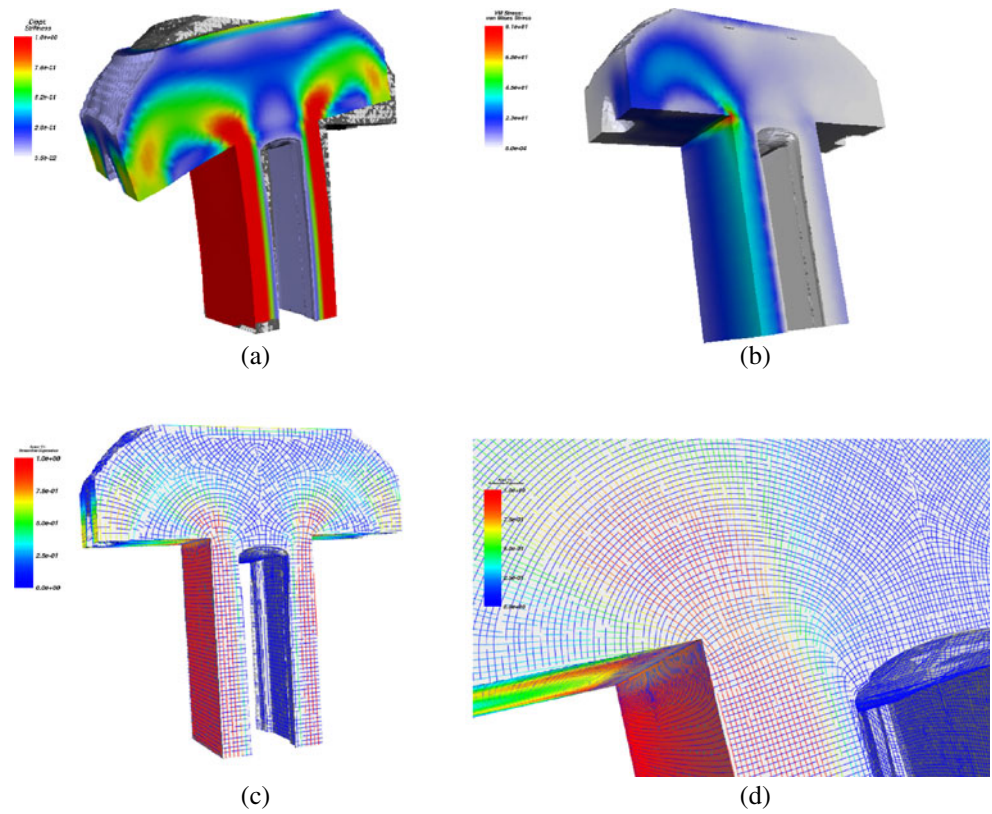
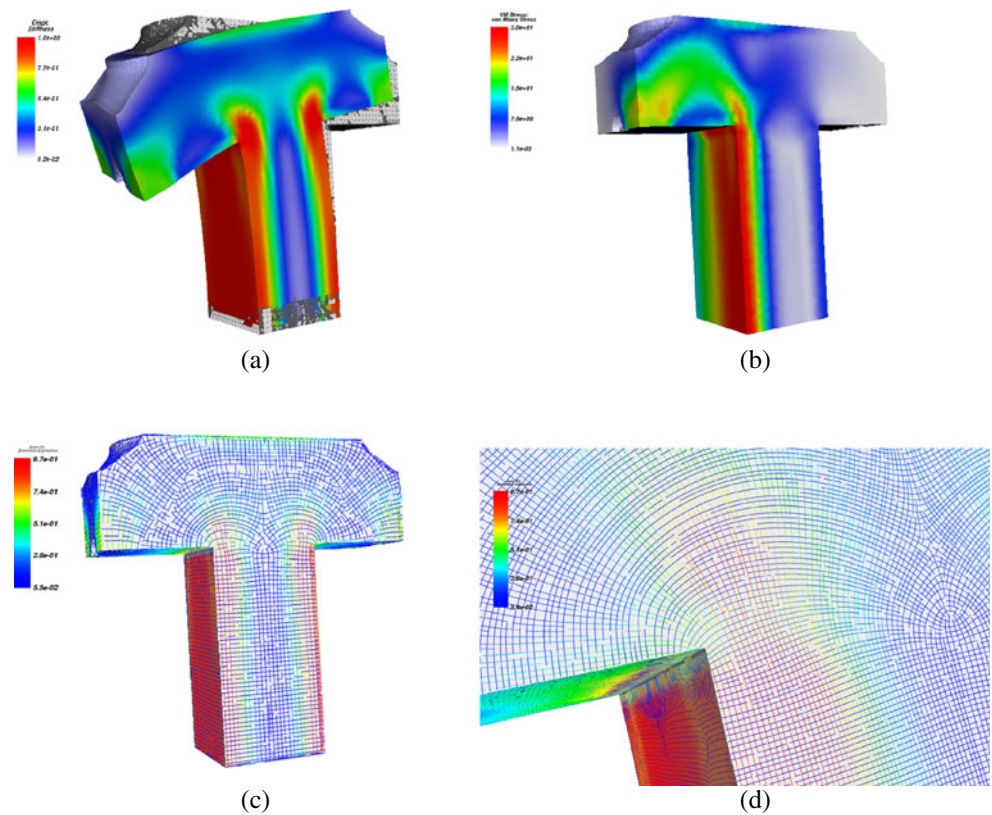


**Fig. 10** Problem TC11-s4 with stress constraints: **a** material density & deformed geometry (first load case); **b** stress distribution—active set; **c** principal material orientation; **d** material orientation (zoom)



stress (mid-left) and zoom on the stress at the re-entrant corner (mid-right) and, finally, the distribution of  $\rho$  for the stress constrained problem (bottom-left) and the corresponding stresses (bottom-right). We can see, as expected, that the stress concentration was removed by a change in the *geometry* of the optimal structure; the re-entrant corner is replaced by a smooth circular “hole”. Notice that we only consider the VTS problem, not a 0–1 material. Hence this circular “hole” does not have a distinct boundary. For isotropic material, the stress is given by a function  $c(\phi)r^{-1/2}$  where  $(r, \phi)$  are the polar coordinates centered at the corner. In order to eliminate this singularity (to make the stress function locally constant), we have to multiply this function by  $\rho(r, \phi) = \bar{c}(\phi)r^{1/2}$  with some suitable  $c(\phi)$ . Hence, as we approach the corner, the density will go to zero as square root of 2 and thus will not be equal to zero even very close to the corner. This effect is further emphasized by the fact that we are only using approximate (and thus finite) values of the stress obtained by the discretization.

Again, we used four iterations of the penalty algorithm, so four calls to PENSOP. The final objective value was 0.3506. The maximum stress value in each iteration was, respectively, 2.68, 2.40, 2.23, and 2.12. The total CPU time was 24 min 1 s and the cumulated number of iterations was 189. (Unconstrained problem: 144 iterations, 12 min 9 s, maximal stress value 5.7 and objective value 0.3401.)

**Example 3** (TC12-s2, FMO) In order to demonstrate the ability of the code to solve three-dimensional problems, we consider a three-dimensional L-shaped geometry, problem TC12-s2 from the PLATO-N library. We only consider the FMO formulation. The design domain clamped at the bottom is loaded by a vertical load on the right hand side of the structure (see Fig. 5). The design space is discretized by approximately 12.000 finite elements. In both, the unconstrained as well as the constrained case, we have used the compliance bound of 19.0. We first minimize the compliance of the structure without stress constraint. The computation time for the unconstrained problem was 56 min and 204 iterations were required. At the optimum the value of the objective was 0.3191 and the highest stress was 8.1290. Figure 6 shows:

- the optimal material density computed by the trace of the material tensor on every element together with the deformation of the body (a);
- the principal material orientation (b);
- the von Mises stress distribution (c).

As expected, stress concentration appears along the edge of the re-entrant corner (see Fig. 6c).

The results with penalized stress constraints for the upper stress bound  $s_\sigma = 2.5$  are shown in Fig. 7. Using the same

compliance bound we obtained a slightly higher objective value of 0.3853 (see Fig. 7a). On the other hand, the stress concentration was completely avoided (see Fig. 7c)—the highest stress value was 2.5099. Moreover, Fig. 7d indicates that the stress constraints become active in large areas of the design domain (activity is indicated by the red color). Figure 7b provides an explanation how the stress reduction is achieved: as in the two-dimensional example the material forms an arch like structure close to the sharp edge. The constrained problem was solved in approximately 2 h 27 min, taking 911 iterations.

**Example 4** (TC11-s4, FMO) Finally, we solve a large-scale three-dimensional example with several load cases, to simulate the behaviour of the code on real-world examples. We consider problem TC11-s4 from the PLATO-N library—a T-bar structure with four load cases discretized by 40.000 finite elements. To solve the FMO problem without stress constraints, the PENSOP code needed approximately 2 h and 30 min (using 151 iterations). The stress constrained problem (with 840.000 design variables and 40.000 stress constraints) was solved in about 36 h and 40 min (using 608 iterations). Applying a stress bound of 30, the maximal stress could be reduced from 90.9 (unconstrained case) to 30.02 (constrained case). On the other hand, the objective function value grew from 0.325 (unconstrained case) to 0.425 (constrained case). As in the previous examples, the compliance of the structure was the same in both cases. Figure 8 shows the initial structure and Figs. 9 and 10 the results.

## References

- Achtziger W, Kanzow C (2007) Mathematical programs with vanishing constraints: optimality conditions and constraint qualifications. *Math Program* 114(1):69–99
- Alizadeh F, Eckstein J, Noyan N, Rudolf G (2008) Arrival rate approximation by nonnegative cubic splines. *Oper Res* 56:140–156
- Bendsøe M, Sigmund O (2002) *Topology optimization. Theory, methods and applications*. Springer, Heidelberg
- Bendsøe MP, Guedes JM, Haber R, Pedersen P, Taylor JE (1994) An analytical model to predict optimal material properties in the context of optimal structural design. *J Appl Mech* 61:930–937
- Bletzinger KU (1993) Extended method of moving asymptotes based on second-order information. *Struct Multidisc Optim* 5(3): 175–183
- Cheng G, Jiang Z (1992) Study on topology optimization with stress constraints. *Eng Optim* 20:129–148
- Ciarlet PG (1978) *The finite element method for elliptic problems*. North-Holland, Amsterdam
- Duysinx P, Sigmund O (1997) New developments in handling stress constraints in optimal material distribution. In: *Proceedings of the 7th AIAA/USAF/NASA/ISSMO symposium on multidisciplinary analysis and optimization*, St. Louis, Missouri, pp 1501–1509
- Fleury C (1989) Efficient approximation concepts using second order information. *Int J Numer Methods Eng* 28:2041–2058

- Kirsch U (1990) On singular topologies in optimum structural design. *Struct Multidisc Optim* 2:39–45
- Kočvara M, Stingl M (2007) Free material optimization: towards the stress constraints. *Struct Multidisc Optim* 33(4–5):323–335
- Le C, Norato J, Bruns TE, Ha C, Tortorelli DA (2010) Stress-based topology optimization for continua. *Struct Multidisc Optim* 41(4):605–620
- Petersson J (1996) On stiffness maximization of variable thickness sheet with unilateral contact. *Q Appl Math* 54:541–550
- Rozvany GIN (2001a) Aims, scope, methods, history and unified terminology of computer-aided topology optimization in structural mechanics. *Struct Multidisc Optim* 21:90–108
- Rozvany GIN (2001b) Stress ratio and compliance based methods in topology optimization—a critical review. *Struct Multidisc Optim* 21(2):109–119
- Rozvany GIN, Zhou M, Birker T (1992) Generalized shape optimization without homogenization. *Struct Optim* 4:250–252
- Stingl M, Kočvara M, Leugering G (2009a) A new non-linear semidefinite programming algorithm with an application to multidisciplinary free material optimization. In: Kunisch K, Leugering G, Sprekels J, Tröltzsch F (eds) *Optimal control of coupled systems of partial differential equations*. International series of numerical mathematics, vol 133. Birkhäuser, Cambridge, pp 275–295
- Stingl M, Kočvara M, Leugering G (2009b) A sequential convex semidefinite programming algorithm with an application to multiple-load free material optimization. *SIAM J Optim* 20(1):130–155
- Svanberg K (1987) The method of moving asymptotes—a new method for structural optimization. *Int J Numer Methods Eng* 24:359–373
- Svanberg K (2002) A class of globally convergent optimization methods based on conservative separable approximations. *SIAM J Optim* 12:555–573
- Waki H, Kim S, Kojima M, Muramatsu M (2006) Sums of squares and semidefinite programming relaxation for polynomial optimization problems with structured sparsity. *SIAM J Optim* 17:218–242
- Yang RJ, Chen CJ (1996) Stress-based topology optimization. *Struct Multidisc Optim* 12(2–3):98–105
- Zhou M, Rozvany G (1992) DCOC: an optimality criteria method for large systems. Part I: theory. *Struct Multidisc Optim* 5(1–2):12–25
- Zhou M, Rozvany G (1993) DCOC: an optimality criteria method for large systems. Part II: algorithm. *Struct Multidisc Optim* 6(4):250–262
- Zillober C (2001) Global convergence of a nonlinear programming method using convex approximations. *Numer Algorithms* 27(3):256–289
- Zowe J, Kočvara M, Bendsøe M (1997) Free material optimization via mathematical programming. *Math Program, Ser B* 79:445–466